

UNIVERSIDADE ESTADUAL DE CAMPINAS  
SISTEMA DE BIBLIOTECAS DA UNICAMP  
REPOSITÓRIO DA PRODUÇÃO CIENTÍFICA E INTELECTUAL DA UNICAMP

**Versão do arquivo anexado / Version of attached file:**

Versão do Editor / Published Version

**Mais informações no site da editora / Further information on publisher's website:**

<https://www.sciencedirect.com/science/article/pii/S0304885316322648>

**DOI: 10.1016/j.jmmm.2017.01.071**

**Direitos autorais / Publisher's copyright statement:**

©2017 by Elsevier. All rights reserved.

DIRETORIA DE TRATAMENTO DA INFORMAÇÃO

Cidade Universitária Zeferino Vaz Barão Geraldo

CEP 13083-970 – Campinas SP

Fone: (19) 3521-6493

<http://www.repositorio.unicamp.br>



# Domain wall propagation tuning in magnetic nanowires through geometric modulation



L.C.C. Arzuza<sup>a,b,\*</sup>, R. López-Ruiz<sup>a</sup>, D. Salazar-Aravena<sup>a,c</sup>, M. Knobel<sup>a,d</sup>, F. Béron<sup>a</sup>, K.R. Pirota<sup>a</sup>

<sup>a</sup> Instituto de Física Gleb Wataghin, Universidade Estadual de Campinas, 13083-859 Campinas (SP), Brazil

<sup>b</sup> Universidad de la Costa, Departamento de Ciencias Naturales y Exactas, Calle 58 No. 55-66, Barranquilla, Colombia

<sup>c</sup> Departamento de Física, Facultad de Ciencias, Universidad de Tarapacá, 1000007 Arica, Chile

<sup>d</sup> Brazilian Nanotechnology National Laboratory, Centro Nacional de Pesquisa em Energia e Materiais (CNPEM), 13083-970 Campinas (SP), Brazil

## ARTICLE INFO

### Article history:

Received 25 September 2016

Received in revised form 4 January 2017

Accepted 25 January 2017

Available online 28 January 2017

## ABSTRACT

The magnetic behavior of nickel modulated nanowires embedded in porous alumina membranes is investigated. Their diameters exhibit a sharp transition between below (35 nm) and above (52 nm) the theoretical limit for transverse and vortex domain walls. Magnetic hysteresis loops and first-order reversal curves (FORCs) were measured on several ordered nanowire arrays with different wide-narrow segment lengths ratio and compared with those from homogenous nanowires. The experimental magnetic response evidences a rather complex susceptibility behavior for nanowires with modulated diameter. Micromagnetic simulations on isolated and first-neighbors arrays of nanowires show that the domain wall structure, which depends on the segment diameter, suffers a transformation while crossing the diameter modulation, but without any pinning. The experimental array magnetic behavior can be ascribed to a heterogeneous stray field induced by the diameter modulation, yielding a stronger interaction field at the wide extremity than at the narrow one. The results evidence the possibility to control the domain wall propagation and morphology by modulating the lateral aspect of the magnetic entity.

© 2017 Elsevier B.V. All rights reserved.

## 1. Introduction

Magnetic nanowire arrays were initially envisaged as potential candidates for high density magnetic recording, where the magnetization of each wire would represent a bit of information [1]. Recently, a novel approach was proposed for a magnetic random-access memory, where the moving domain wall along the wire constitutes the binary element in a race-track memory [2]. This approach requires the creation and manipulation of domain walls in a controlled way. The geometric handle of the domain wall movement, combined with domain walls moved by spin polarized current pulses, can represent important advances in the development of novel devices [3]. Generally speaking, the presence of inhomogeneities, such as modulation of the diameter along the wire, can play a major role on the control of the domain walls pinning/depinning processes. In this respect, some open questions related to domain wall dynamics still need to be investigated. The influence on the domain wall mobility due to the wire intrinsic shape anisotropy [4,5], dipolar interactions and domain wall fea-

tures, induced by wire diameter, represents crucial information. Magneto-optical Kerr effect and micromagnetic simulations have been extensively used to investigate the fundamental mechanisms that limit the domain wall mobility, for example, the pinning effect created by localized stray field [6] in Y junctions [7] or in patterned Co wires [8], sometimes revealing complex walls with different substructures [9]. Because of the size involved, the low-cost preparation and the simple geometrical modulation, nanowires prepared in porous alumina membranes constitute an ideal system to study these processes.

Here, we present a comprehensive magnetic study, including experiments and micromagnetic simulations, on a simple modification of the wire geometry: a bottleneck that yields to two-segment nanowires presenting different diameters in each segment. Up to now, very few studies on diameter-modulated magnetic nanowires (DMNW) have been reported. For example, in multi-segmented CoFe nanowires, dipolar interactions due to stray fields in the macroscopic samples were found to be quite important to influence the magnetization process [10]. Silica-coated segmented permalloy arrays show a variation in the coercivity and hysteresis shape depending on the diameter transition position [11]. For Ni nanowires with a single modulation along their length, experimental studies showed that arrays present intermediate magnetic properties between narrow and wide nanowires [12],

\* Corresponding author at: Universidad de la Costa, Departamento de Ciencias Naturales y Exactas, Calle 58 No. 55-66, Barranquilla, Colombia. Tel.: +57-5-3362200.

E-mail addresses: [luisarzuza179@gmail.com](mailto:luisarzuza179@gmail.com), [lcosta@cuc.edu.co](mailto:lcosta@cuc.edu.co) (L.C.C. Arzuza).

and that, with both diameters larger than 55 nm, no pinning or susceptibility change was observed, probably due to magnetocrystalline inhomogeneities and thermal fluctuations [13]. On the other hand, theoretical Monte Carlo simulations on a single nanowire revealed that the diameter modulation can induce a susceptibility change in the hysteresis loop, when the domain wall suffers a pinning at the diameter interface [14]. Moreover, a diameter-related modification of the magnetization reversal process was observed, passing from a transverse to vortex wall nucleation for diameter between approximately 45 and 65 nm. Micromagnetic simulations performed on a cone-shaped Ni nanowire and micromagnetic analysis found a similar behavior, where the transverse/vortex transition occurred at a diameter of about 40 nm [15,16].

However, no modulated nanowires in the transverse regime have been experimentally investigated up to now. Therefore, with the aim to deal with extreme cases, we fabricated Ni modulated nanowires with diameter segments above and below the transverse/vortex domain wall formation crossover, respectively. Their magnetic response was studied as a function of the wide segment length. Firstly, we present the synthesis and structural characterization of diameter-modulated Ni nanowires (Section 2). Secondly, we expose the experimental magnetic characterization by means of major hysteresis loops and first-order reversal curve (FORC) diagrams (Section 3), and micromagnetic simulations of isolated and first-neighbors array of nanowires (Section 4). Finally, in order to better understand the experimental behavior, simulations of a macroscopic array using the physical model of hysterons [17] are used (Section 5). It allows to elucidate interesting aspects about the hysteresis reversal modes and the collective response influence on the domain wall shape and propagation in these magnetic entities.

## 2. Sample details

Nanowires were produced embedded in the hexagonal honeycomb structure of porous alumina membranes by means of a template-assisted method [18]. The nanowires diameter modulation was achieved through the variation of the membrane pores diameter. This protocol, named three-step anodization method, has been specifically developed to easily obtain high quality two-segment nanowire arrays. It is based on the well-known two-step anodization technique in mild conditions [19–22] to first obtain a 35 nm diameter pores alumina array with a hexagonal pattern (DC voltage of 40 V in oxalic acid at 3 °C) (Fig. 1(a)). The pores are widened through chemical etching with  $H_3PO_4$  (Fig. 1(b)), before a third anodization, keeping constant the parameters, produces once more 35 nm pores at the alumina membrane bottom (Fig. 1(c)).

The pores geometry was controlled by taking into account a pores growth rate of 2.5  $\mu\text{m}/\text{h}$  and a pore diameter widening rate of 0.5 nm/min ( $T = 22^\circ\text{C}$  and 8.5% (w/w) concentration). It is worth noting that, because the same mild anodization parameters are used throughout the process, the third anodization pores grow in the extension of the second anodization ones, while the inter-pore distance is kept constant (around 105 nm) (Fig. 1(d)), unlike in the hard/mild anodization method [12]. The hexagonal pattern remains through the alumina membrane, with pores of 35(2) nm diameter overhung by pores of 52(2) nm, respectively called narrow and wide segments (Fig. 1(e, f)). The diameter modulation transition is relatively abrupt, extending over a 40(2) nm-long region.

In order to focus on the consequences of the diameter variation on the array magnetic behavior, the pores were filled with Ni pulsed electrodeposition following Refs. [20,21], achieving a pore filling factor of almost 100%. Three different geometries of

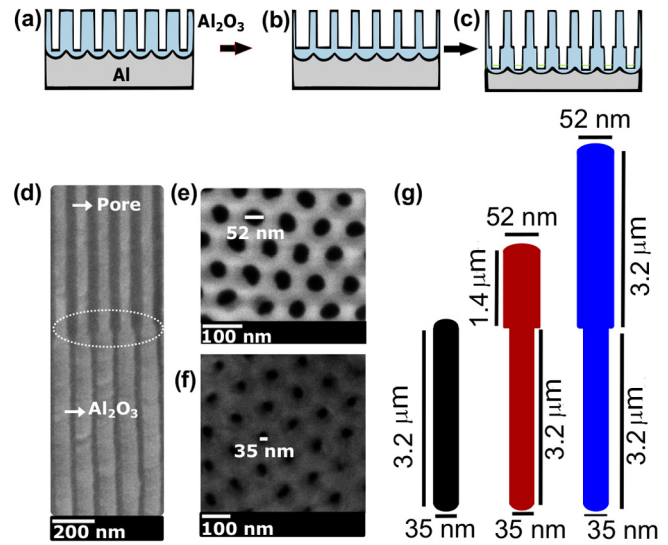


**Fig. 1.** (a–c) Preparation scheme of DMNW arrays, via the three-step anodization process. (d) Alumina template cross-section view of the diameter transition region (encircled). Top (e) and bottom (f) views of a DMNW alumina template array, exhibiting different pore diameters. (g) Schematic representation of the investigated nanowire geometries (not at scale). Left to right: reference, same-volume and same-length nanowires.

nanowire array were compared, keeping the narrow segment identical (3.2  $\mu\text{m}$ -long) (Fig. 1(g)). A uniform nanowire array, solely composed of the narrow segment, was used as reference. Two modulated diameter arrays were fabricated: a same-volume segments (approx.  $3 \times 10^6 \text{ nm}^3$ ) and a same-length segments geometries. The pore diameters were specifically chosen to study nanowire segments above and below the critical diameter for domain wall types nucleated in Ni nanowires.

## 3. Experimental magnetic characterization

The FORC technique is related to the Preisach model, where the magnetic behavior arises from a collection of different irreversible processes, called hysterons [23]. A hysteron is a purely irreversible operator characterized by a squared hysteresis with coercivity  $H_c$  and a field shift  $H_u$ . The FORC technique represents an experimental way to get access to more information about the hysteretic behavior of a system, in comparison to the major hysteresis curve, since it allows to decouple the individual nanowire coercivity from the interaction field among the nanowires [24]. However, it is important to stress out that for most magnetic systems, such as nanowire arrays, it does not yield the Preisach hysteron distribution, since its congruency requirement is not met [23]. Therefore, experimental FORC results need to be carefully interpreted, using for instance the physical analysis model [17], which will be described in details in Section 5.

The FORC protocol is based on the acquisition of several minor loops, i.e., FORCs, from a reversal field  $H_r$  until the saturation field, measuring the magnetization in regular field steps  $\Delta H$  [23]. The second-mixed derivative of the resulting magnetization  $M(H, H_r)$  gives the FORC distribution. Its contour plot diagonal axes, namely, the coercive field axis  $H_c = (H - H_r)/2$  and the interaction field axis  $H_u = -(H + H_r)/2$ , are related to the Preisach hysterons characteristics. In the typical case where the nanowires present similar coercivity and are submitted to a mean-type demagnetizing interaction field ( $H_{int} = kM/M_s$ , where the interaction field constant  $k$  is negative), a proper parametrization permits to extract these two values from the FORC diagram. The obtained distribution is elongated along the  $H_u$  axis, proportionally to the interaction field at

saturation, and located on the  $H_c$  coordinate equal to the nanowire coercivity [24]. For other cases, an adequate parametrization is required, especially since FORC results may not be intuitive.

Both major hysteresis loops and FORCs were measured with an applied magnetic field  $H$  along the wires axis on a commercial vibrating sample magnetometer (VSM) at room temperature. Experimental magnetic characterization of the reference Ni nanowire array matches results previously obtained in similar geometry [25]. Major hysteresis curve presents a large squareness ( $>0.9$ ) with a typical coercivity of around 550 Oe (Fig. 2(a)). Its magnetic susceptibility emphasizes its slightly sheared behavior, due to the dipolar interaction field among nanowires, but symmetrical with respect to its maximum (Fig. 2(b)). Finally, its FORC distribution exhibits an expected wishbone shape (Fig. 3(a)), characteristic of

systems with coercivity distribution submitted to demagnetizing interaction field [26].

The most notable difference between major hysteresis loops is the decrease of the magnetic susceptibility as the wide segment length increases (Fig. 2(b)), which could be associated to an increase of the dipolar interaction field. The elongation of the FORC distribution along the  $H_u$  axis seems to confirm this hypothesis (Fig. 3) [17]. Therefore, since the nanowire interdistance remains constant, the larger magnetic volume and surfaces created by the addition of the wide segment increase the dipolar interactions.

However, some important features of the DMNW arrays magnetic characterization differ from the obtained results for the reference array. First, the susceptibility curves appear more asymmetrical with respect to their maximum as the wide segment elongates (Fig. 2(b)), suggesting that the nanowire magnetization reversal does not remain constant during the array magnetization reversal, i.e., that it may depend on the magnetic state of the whole array. Furthermore, the position of the susceptibility maximum does not coincide anymore with the coercive field of DMNW arrays. The longer the wide segment, the susceptibility maximum arises at magnetic field values higher than the coercive one.

Second, the DMNW arrays FORC diagrams exhibit a characteristic curvature (see dashed lines on Figs. 3(b, c)). FORC distribution of systems submitted to a mean demagnetizing interaction field will appear as a straight distribution, parallel to the  $H_u$  axis, for identical hysterons [17]. Introducing a coercivity distribution to the system hysterons leads to the typical wishbone shape, as exhibited by the reference array, where the extended distribution is slightly tilted counterclockwise in respect to the  $H_u$  axis. This effect can be understood as the softer hysterons will reverse before the harder ones.

The FORC distribution curvature obtained for DMNW arrays appears relatively symmetric with respect to the  $H_c$  axis. This feature could arise from a system where the order of the hysterons reversal follows the scheme: soft ones, then harder hysterons, and finally soft ones again, for example, in a system where the hysterons coercivity is changing depending of the system magnetization state. Another possible explanation is that the distribution curvature comes from an apparent coercivity variation, created by a more complex interaction field than a mean one, due to the diameter modulation. In both DMNW cases, the FORC distribution extension on  $H_c$  axis was not considered thereafter, since it is assumed to originate from the interaction field spatial non-uniformity due to the macroscopic sample border, the interaction field being weaker near the borders and stronger in the array center [27].

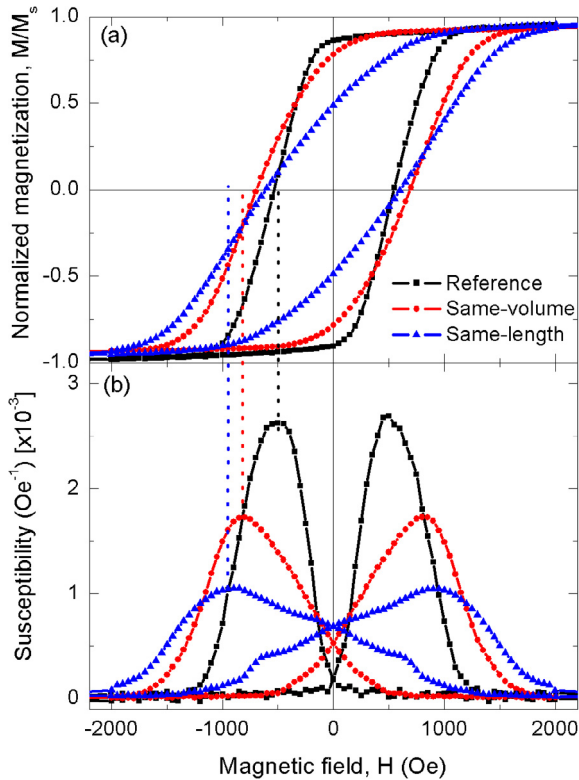


**Fig. 2.** Experimental magnetization (a) hysteresis and (b) susceptibility curves. Dotted vertical lines indicate the susceptibility maximum positions.

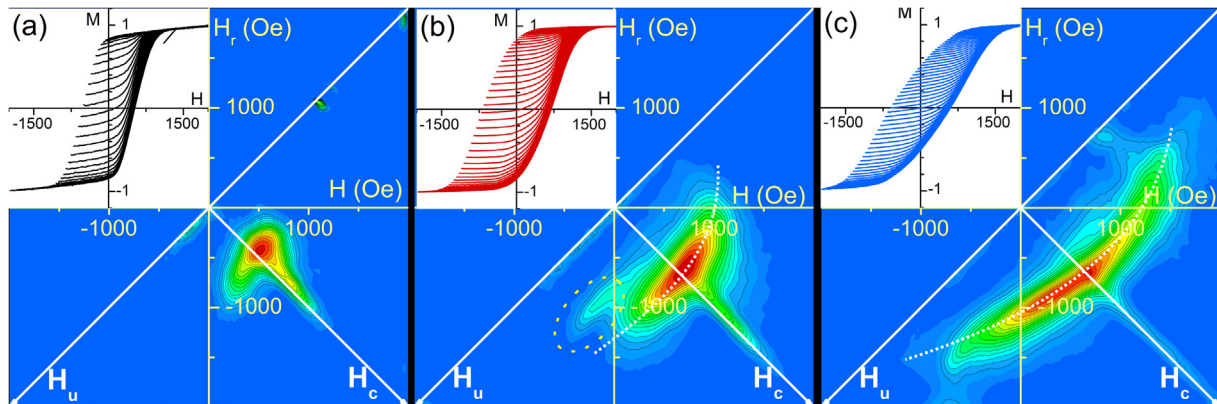


**Fig. 3.** Experimental FORC diagrams of the (a) reference (b) same-volume and (c) same-length nanowire arrays. The color scale ranges from blue to red, for null to maximum distribution value. Insets: Respective experimental FORCs. White dashed curves emphasize the FORC distribution curvature for modulated nanowire arrays. The presence of the additional distribution encircled on (b) is discussed in Section 5.



Finally, both major hysteresis curves (Fig. 2(a)) and FORCs (insets of Figs. 3(b, c)) of DMNW arrays exhibit a smooth behavior. While a domain wall pinning should yield a staircase magnetization curve for a single nanowire, two features may prevent the identification of this behavior on magnetization curves from large nanowire arrays. First, the nanowire reversal does not happen simultaneously due to the demagnetizing interaction field [28]. The second characteristic is the geometrical distribution among nanowires, yielding different pinning field values. Therefore, the domain wall pinning would not happen simultaneously among the nanowires in the array, leading to magnetization curves without plateau. In this case, it may be impossible to distinguish between a domain wall pinning and a still non-reversed nanowire, both from major hysteresis curves and FORCs. However, one could assume that FORC diagram may represent a tool where domain wall pinning signature could be distinguished. Considering each nanowire as an entity where the total reversal occurs in two steps with different reversal field values (nucleation and depinning fields), it would appear as two distinct FORC distributions, both elongated due to the interaction field, but with different  $H_c$  positions.

#### 4. Micromagnetic simulations

Despite the observations that the introduction of a diameter modulation modifies the nanowire array magnetostatic behavior, the macroscopic experimental results do not resolve the microscopic processes occurring during the nanowire magnetization reversal. Therefore, in order to investigate the theoretical domain walls dynamics and the existence of a pinning at the nanowire segments junction, as well as the effects of the dipolar interaction field on the magnetization reversal in our systems, we have performed micromagnetic simulations using the public-domain license OOMMF software [29]. The Landau–Lifshitz–Gilbert equation was solved, in absence of temperature, for a magnetic field applied along the nanowire axis (z-axis). For comparison purposes, we also simulated a wide homogenous nanowire (3.2  $\mu\text{m}$ -long, 50 nm of diameter) in addition to the three nanowire geometries. We studied the consequences of the interaction field by comparing the results obtained for single nanowire with ones for an array. For computational time reasons, we limited the array to first neighbors, i.e., seven nanowires in hexagonal arrangement with 110 nm interwire distance.

For the calculations, we used nickel parameters of stiffness constant  $A = 9 \times 10^{-12} \text{ J/m}$  and saturation magnetization  $M_s = 4.8 \times 10^5 \text{ A/m}$ . As most important anisotropy contribution comes from the nanowire shape, we neglected the magneto crystalline anisotropy. The damping constant was fixed to  $\alpha = 0.5$ , which allows the program to converge in a reasonable number of iterations. To ensure the exchange interaction among magnetic moments, all cell size dimensions must be lower than the Ni exchange length defined by  $l_{ex} = \sqrt{2A/\mu_0 M_s^2} = 7.72 \text{ nm}$ , where  $\mu_0$  is the vacuum permeability. We considered magnetic moment cell sizes of  $1 \times 1 \times 5 \text{ nm}^3$  and  $2.5 \times 2.5 \times 10 \text{ nm}^3$  for single and array geometries, respectively. For the array, we chose to slightly increase the cell size along the z axis to execute the simulations in a reasonable time. All simulations were started with an initial uniform magnetization configuration along the nanowire axis and under a magnetic field of 2000 Oe. The applied field is then decreased until  $-2000 \text{ Oe}$  in steps of 10 Oe.

##### 4.1. Single nanowires

It has been theoretically suggested that the magnetization reversal mechanisms of homogeneous nanowires were coherent and curling modes [30–32]. On the other hand, micromagnetic simulations showed that the magnetization reversal can occur by

domain wall nucleation–propagation in two different reversal modes, known as the transverse and the vortex wall modes [15]. From our results, we observed that the magnetization reversal mode for single homogeneous nanowires of 35 nm and 50 nm diameter, both 3.2  $\mu\text{m}$ -long, is via nucleation and propagation of transverse and vortex domain walls, respectively (see [Supplemental Material A and B](#)). In both cases, the domain walls start to propagate from both ends towards the nanowire center. These results are in agreement with the ones expected for nickel homogeneous wires of similar diameter [15,16].

The micromagnetic simulations yield a similar process for the magnetization reversal of the single DMNWs, with domain walls nucleating at the wire extremities. Therefore, no nucleation was observed in the wide-narrow transition zone, in contrast to Refs. [11,14]. During the whole magnetization reversal of both DMNWs, the domain wall present in each nanowire segment depends on its diameter, as in Refs. [14,15,33] (Fig. 4). As expected, the narrow segment exhibits a transverse domain wall that precesses when propagating. The wide segment, on the other hand, does not present a pure vortex domain wall, as in the complete wide nanowire. It is a more complex structure, which we named helicoidal vortex domain wall and is described in details in [Appendix A](#).

The reversal sequence is analogous for both DMNWs (see [Supplemental Material C and D](#)): (1) A helicoidal vortex domain wall nucleates first at the wide segment extremity, followed by a transverse domain wall at the narrow segment extremity. (2) They begin to propagate towards the wire center. (3) Finally, because the helicoidal vortex wall moves faster than the transverse one, as already observed [16], the wide segment is completely reversed first. When the helicoidal vortex domain wall reaches the transition region, it transforms itself into a transverse wall, as in [15]. (4) It further continues its propagation until completing the nanowire magnetization reversal, without pinning in the transition zone (Fig. 5). The helicoidal vortex domain wall nucleation field

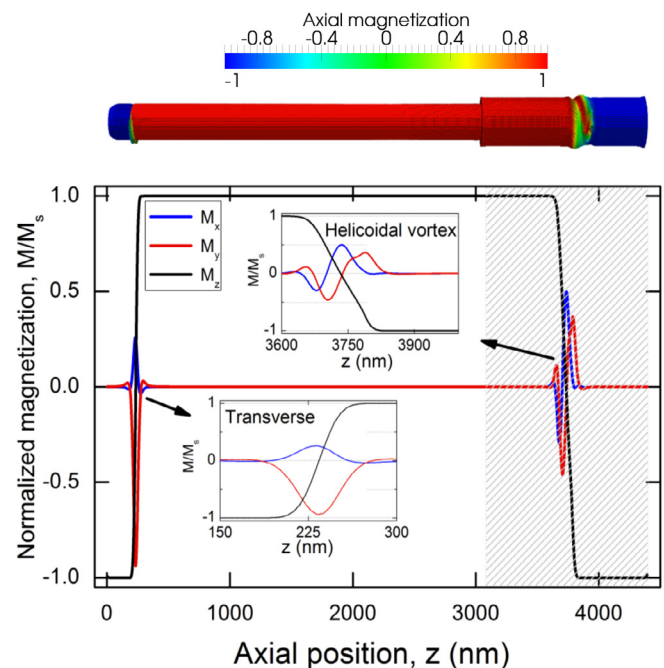


**Fig. 4.** Representation of the simulated magnetization during the reversal of the same-volume DMNW ( $H = -1460 \text{ Oe}$ ), exhibiting a transverse domain wall in the narrow segment and a helicoidal one in the wide segment. Top: three-dimensional representation of the axial magnetization. Bottom: plot of the radial ( $M_x$  and  $M_y$ ) and axial ( $M_z$ ) magnetization components as function of the axial position. The wide segment is delimited by the hatched section. Insets: Zoom on the domain wall regions.

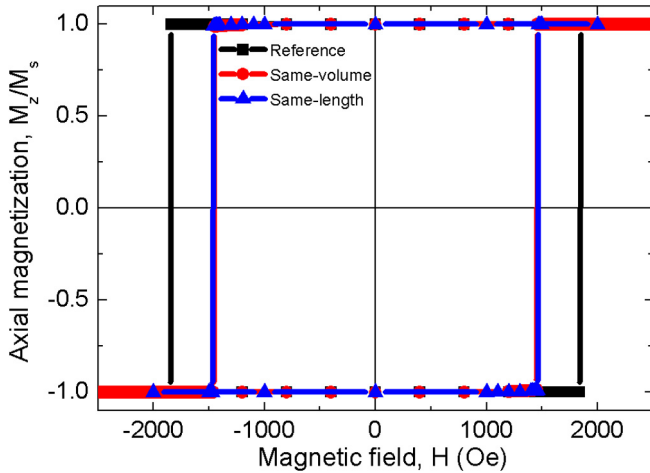


**Fig. 5.** Simulated hysteresis curves for narrow reference single nanowire, as well as DMNW ones.

(−1460 Oe) is identical for both DMNWs geometry, and corresponds to the vortex domain wall nucleation field for the wide homogenous nanowire. However, we observed that, for the same-volume geometry, the domain wall remains at the nanowire extremity before initiating to propagate, while it begins its movement right after its creation for the same-length nanowire. Therefore, our simulated results show that for single nanowire, the diameter modulation does not produce domain wall pinning, but induces a transformation in the magnetization reversal mode, when the nanowire diameters involved are below and above the critical limit, as well as modifies the vortex domain wall structure.

The demagnetizing field ( $H_d$ ) around the nanowires was also extracted from the micromagnetic simulations. In the saturation state, the reference geometry exhibits a negative (i.e. opposite to the magnetization) axial field almost negligible near the nanowire center but rather intense near the extremities (Fig. 6(a)), in agreement with what observed in Ref. [34] and that explains the domain wall nucleation localization. The addition of a wide segment considerably changes the field behavior along the DMNW

(Figs. 6(b, c)). The combination of wide and narrow nanowire segments yields a demagnetizing field that is the sum of each individual segment demagnetizing field. Since the one arising from the wide segment is larger, it creates an abrupt positive to negative field transition at the segments junction. The presence of the positive magnetic field is assumed to explain the absence of domain wall nucleation at the junction. Finally, note that the wide segment increases the field intensity around its extremity, in comparison to around the narrow segment one, which may affect the magnetization reversal of an array of several nanowires (inset of Fig. 6(a)).

#### 4.2. First-neighbors nanowire arrays

The consequences of a dipolar interaction field on the nanowire arrays magnetization reversal mechanisms were investigated through micromagnetic simulations of first-neighbors arrays, as performed in the Ref. [35]. Both homogeneous and diameter-modulated single nanowires exhibit a square hysteresis curve, in agreement with the observed domain wall nucleation-propagation mechanism without pinning (see Fig. 5). On the other hand, their array magnetization reversal occurs by steps. One can observe from the hysteresis curves that the magnetization values during the reversal are all multiples of the nanowires number in the array (Fig. 7). This suggests that the nanowires remain monodomain at equilibrium, pointing either upward or downward, while their reversal field depends on the present demagnetizing interaction field. Similar staircase hysteresis curve, perceptible due to the small amount of simulated wires, has been experimentally obtained for row of few microwires [36]. For both reference and DMNW systems, the array exhibits a lower coercivity than the single nanowire, due to the non-uniform interaction field. It also expands the field interval on which the magnetization reversal occurs [37]. For the same-volume array, this field interval is approximately the double than for the reference array (60 Oe vs 30 Oe), in qualitative agreement with the experimental results that indicate a stronger interaction field in the DMNW array.

More interesting is the simulated magnetization reversal sequence. When arranged in array, the reference geometry reversal is similar to the one observed in single wires, i.e. nucleation–

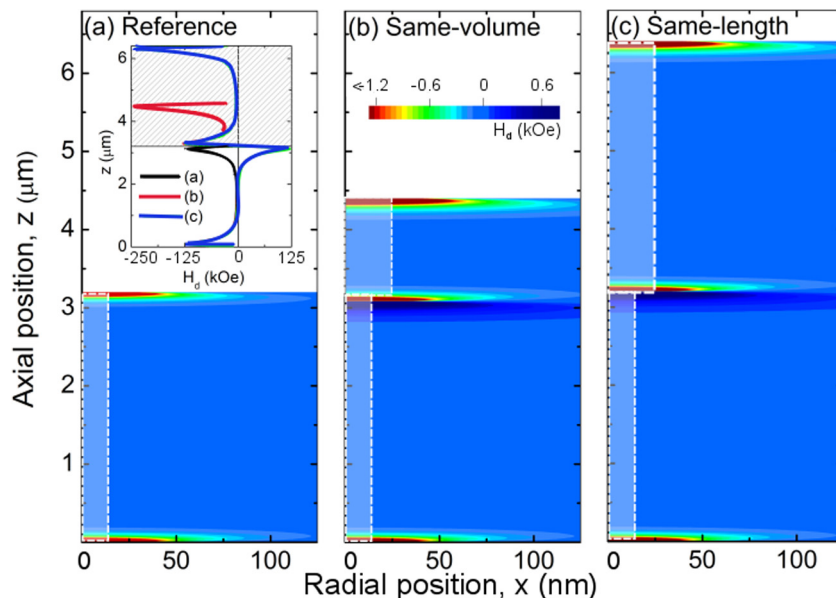


**Fig. 6.** Axial cross-section of the z-component of the demagnetizing field around single axially saturated nanowire (represented in superposition), obtained by micromagnetic simulations. (a) Reference (b) Same-volume (c) Same-length nanowires. The DMNWs lower limit field scale has been limited to −1.2 kOe, in order to enhance the low field behavior. In both cases, it reaches −2.5 kOe. (a) Inset: Demagnetizing field cross-section taken at the first-neighbors distance position (110 nm). The wide segment is delimited by the hatched section.

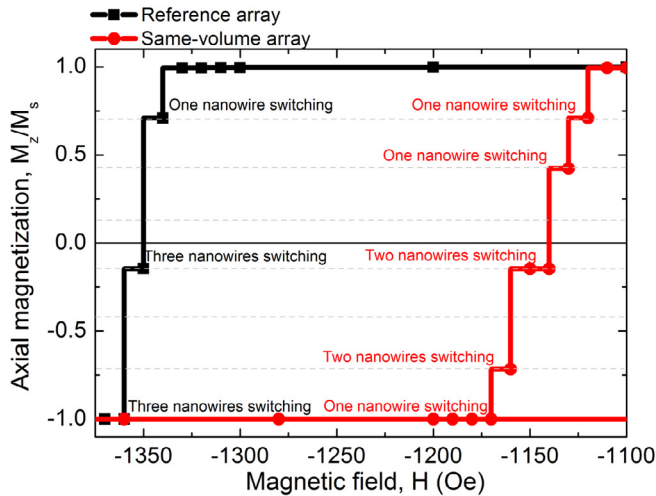


**Fig. 7.** Simulated hysteresis curves for reference (black) and same-volume DMNW (red) first-neighbors arrays of nanowires (negative field part shown). Dashed lines indicate 1/7th magnetization amplitude multiples.

propagation of transverse domain wall from wire extremities (see [Supplemental Material E](#)). After a single nanowire from the border reverses, the inversion continues through the array, via groups of three nanowires, until reaching the opposite side. The magnetization reversal observed in DMNW arrays does not differ significantly, in the sense that it is mainly a successive reversal of few nanowires, by groups of one or two, also crossing the array from one side to the other (see [Supplemental Material F](#)). However, the main consequence of the dipolar field in this case is that the domain wall nucleation solely occurs at one extremity, the wide one, before propagating throughout the whole nanowire. This symmetry breaking can be explained by the magnetic field value created by one neighbor nanowire. This value at the wide extremity being twice the value at the narrow one (see [Fig. 6\(a\)](#) inset), it favors a nucleation at the wide extremity of a nanowire next to a still non-reversed one.

## 5. Discussion

Since micromagnetic simulations are limited to arrays of few nanowires, while dipolar field is a long-range interaction, we used the physical analysis model to obtain the simulated behavior of large arrays and compare it with experimental results. Its objective is to simulate the magnetic behavior of given hysterons (which are physically meaningful) in the presence of an interaction field, according to an applied field sequence (major hysteresis curve, FORCs, etc.) [17]. For each applied field, a hysteron is randomly chosen to reverse state, among those where the total field ( $H + H_{int}$ ) would favor an inversion. The new total field is then calculated, and hysteron reversal occurs until no further reversal is favored. All simulations were performed in a quasi-static mode, calculating the equilibrium state of 1000 hysterons with steps of 1 Oe. Both parameters in the physical analysis model, i.e. the physically meaningful hysterons (hysteresis curves of magnetic elements) and kind of interaction field, were taken from the micromagnetic simulations results. On the other hand, numerical values of these parameters were extracted from the experimental FORC diagrams.

For all geometries, we associated a squared hysteresis curve to the magnetization reversal of each nanowire, modulated or not, as obtained in [Fig. 5](#). For the reference array, the wishbone FORC distribution suggests an almost uniform magnetization-dependent demagnetizing interaction field, but with a non-negligible coercivity distribution [38]. Therefore, we modeled the interaction field as

a mean one, with negative  $k$  value. The numerical values of average coercivity  $\mu_c$  and standard deviation  $\sigma_c$ , as well as interaction field constant, were extracted from the experimental FORC distribution extremities, following the method presented in [38,39].

On the other hand, the magnetic field produced by DMNW saturated single nanowires is non-uniform (see [Fig. 6](#)), suggesting that the interaction field under which domain wall nucleation could occur at each extremity can differ. We thus modeled the DMNW interaction field as the following: at all times, the squared hysterons are independently submitted to two different mean field interaction constants, both negative, to account for the stronger ( $k_{max}$ ) and weaker ( $k_{min}$ ) interaction fields felt at the wide and narrow segment extremities, respectively. Depending on the system magnetization, either maximum or minimum interaction field could be sufficient to reverse the hysteron, thus mimicking a nanowire reversal by nucleating a domain wall in the wide or narrow segment, depending on the array magnetization state. As a first approximation, we assumed an identical nucleation field at both extremities, despite the single nanowires micromagnetic simulations results. This choice is motivated by the lack of discontinuity around  $H_c$  axis observed on DMNW experimental FORC results (see [Figs. 3\(b, c\)](#)). The method to extract the numerical values from this type of FORC distribution is explained in [Appendix B](#).

Both major hysteresis and susceptibility curves ([Fig. 8](#)), and FORC diagrams ([Fig. 9](#)), obtained through the application of the physical analysis model, agree well with their respective experimental result, for all three investigated geometries. Qualitatively, the DMNW hysteresis curves present an asymmetric susceptibility, which maximum is shifted to higher field than the coercivity, as the wide segment length is increasing. Their corresponding FORC

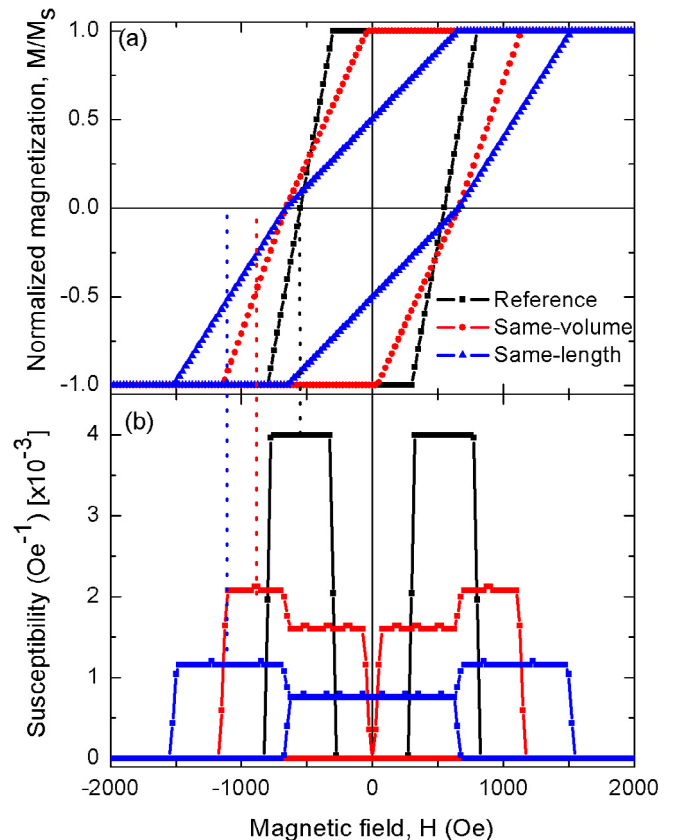


**Fig. 8.** Simulated (a) major hysteresis and (b) susceptibility curves obtained using the physical analysis model. Dotted vertical lines indicate the susceptibility maximum positions.

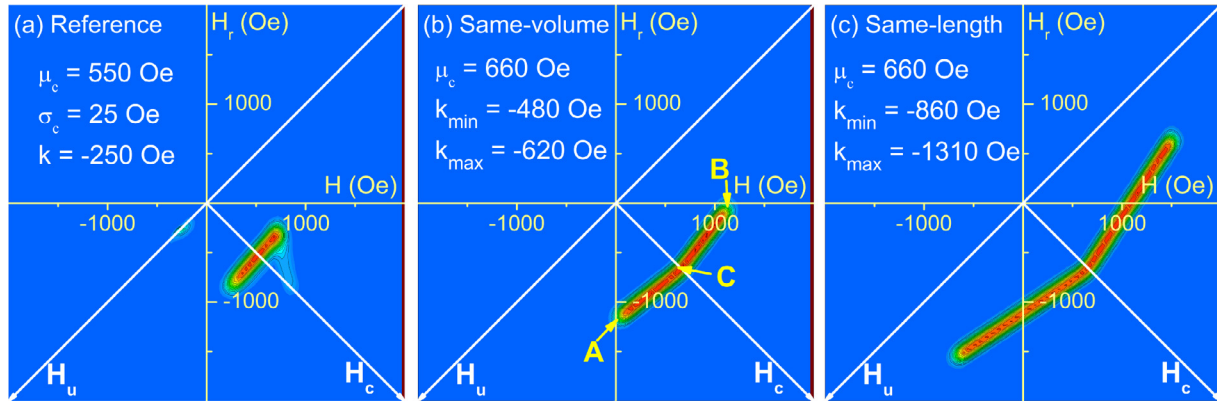


**Fig. 9.** Simulated FORC diagrams of the (a) reference (b) same-volume and (c) same-length nanowire arrays using the physical analysis model. Points A, B and C on (b) represent the FORC distribution characteristic positions used for its parametrization (see Appendix B).

distributions exhibit a bent shape, symmetric with respect of the  $H_c$  axis. Both features directly result from the non-uniform interaction field, proving that experimental curved FORC distributions may not arise from a coercivity variation.

In the physical analysis simulations, a positive magnetization favors a reversal using the greater interaction field constant,  $k_{max}$ , creating the low susceptibility plateau, while the weaker one,  $k_{min}$ , is used under a negative magnetization, thus giving rise to the high susceptibility plateau. Since the susceptibility transition occurs at the coercive field ( $M = 0$ ), it explains the susceptibility maximum shift from the coercivity. The stronger the interaction fields involved, the wider are these plateaus and therefore the observed shift. Similarly, during the FORCs calculation, the hysterons are reversing down with the help of the stronger interaction field, but they come back up using the weaker one, when magnetization is positive, and the opposite occurs for negative magnetization. This switch of reversal field values yields asymmetric hysterons, explaining the bent FORC distributions.

The qualitative agreement between experiments and simulations via physical analysis model suggests that the DMNW array magnetization reversal begins by domain wall nucleation at the wide segment extremity for positive saturation, since the dipolar interaction field is stronger. After sufficient nanowires have been inverting from the wide segment to yield a net negative magnetization, it favors a domain wall nucleation where the dipolar interaction field is now the weakest, which corresponds to the narrow segment extremity. Therefore, the geometrical asymmetry created by the diameter modulation, combined with dipolar interaction field, induces an asymmetry in the magnetic behavior of DMNW arrays. We ascribed the absence of sharp susceptibility plateaus and the FORC distribution curvature in experimental results to the coercivity distribution among nanowires (mainly attributed to diameter distribution) and the interaction field lateral non-uniformity (weaker near the array edges, due to less neighboring nanowires). Additionally, the good agreement obtained with experimental results justifies the assumption of similar nucleation fields at both extremities.

We can quantitatively compare the magnetostatic values used in the physical analysis simulations (see Fig. 9). As expected, the absolute value of the interaction field constants increases with the nanowire volume. Similar to what obtained from array micromagnetic simulations, the same-volume system exhibits a higher interaction field that is more than twice the value for the reference one. However, we observe that the  $k_{min}$  values (and  $k$  for reference array) are not equal, the first one increasing with the wide segment length, unlike to what observed in Fig. 6(a) inset. It is important to note that the interaction field values are extracted from

experimental FORC diagrams, based on a simplified model of identical hysterons submitted to two interaction fields. Other effects, such as the nucleation field difference between the wide and narrow extremity, can interplay in the extracted values. The coercivity value extracted from DMNW experimental FORC distributions corresponds to an individual nanowire switching field. Remarkably, they are identical for the same-volume and same-length geometries, as already observed in micromagnetic simulations of single nanowires (see Fig. 5). Since the effects of the interaction field on the major hysteresis curve coercivity are difficult to quantify, the FORC method, with the help of the parameterization presented in Appendix B, proves its utility and accuracy to probe the coercivity of individual modulated diameter nanowires in an array.

Finally, the same-volume DMNW experimental FORC diagrams exhibits an additional distribution located near the bottom extremity (encircled on Fig. 3(b)). Because this distribution does not appear on the FORC simulations done by means of the physical analysis model, an additional behavior is probably occurring in the real samples. One possibility is that the demagnetizing field created at the segments interface, which did not have been considered in the actual simulation model, also contributes to modify the array reversal behavior. Further experiments need to be performed to clarify this point.

## 6. Conclusions

In order to apply magnetic nanowires for novel magnetic recording devices, it is necessary to fine-tune and manipulate the magnetic domains. One promising strategy is the use of diameter-modulated nanowires. In particular, Ni nanowires embedded in nanoporous alumina template were successfully produced with diameters below and above the transverse/vortex domain wall transition, in order to explore the involved magnetization reversal. We observed, from micromagnetic simulations, that both homogeneous and modulated single nanowires reverse their magnetization through an abrupt jump. However, we noted that homogeneous nanowires reverse their magnetization through a vortex or transverse mode, and the same wall propagates along the full length. On the other hand, for modulated nanowires, the dynamics occurs through two independent magnetization reversal processes: helicoidal vortex wall and transverse mode. Experimental major hysteresis loops in two-segment nanowires show a change in the susceptibility in contrast to homogeneous nanowires, being more evident when the wide/narrow length aspect ratio increases. Analysis via FORC method shows an enhancement of the interaction fields and reveals a non-uniform two-component stray field due to shape modulation. Therefore,



the phenomenological differences between homogeneous and diameter-modulated nanowire arrays behavior can be ascribed to a complex performance in which a non-uniform stray field plays the key role. We believe that the evidences reported in this work contribute to elucidate some fundamental aspects concerning the magnetization reversal of magnetic nanowires, as well as giving some insights on possible ways to further control the domain wall movement within the system.

### Acknowledgments

This work was financially supported by the Brazilian funding agencies FAPESP, CNPq and CAPES, as well as the Chilean CONICYT. We thank the Centro Nacional de Pesquisa em Energia e Materiais (CNPq) for the use of the microscopy facilities in the C2NANO-Brazilian Nanotechnology National Laboratory (LNNano), and the CENAPAD-SP for the use of SGI/Altix ICE and computer facilities. D. S. A. acknowledges Ms. D. Cortés-Ortuño for useful discussions.

### Appendix A. Helicoidal vortex domain wall

Instead of exhibiting a vortex domain wall, as in wide homogeneous single nanowire, micromagnetic simulations yield a more complex domain wall structure for the DMNW wide segment (see Fig. 4). It presents an axial elongation as a screw, which rotates during the domain wall propagation, while the vortex core is following a spiral path (Fig. 10). Similar structure was obtained by Tejo et al. [40], but without being discussed. The net magnetization remains completely axial, as in a vortex domain wall (see Fig. 4 inset). We attribute the particular helicoidal feature to the presence of the transverse domain wall in the narrow segment, since simulated DMNW, constituted of two wide segments of 49 nm and 70 nm, does not present helicoidal, but two vortex domain walls (not shown here). It is already well known that an AC in-plane magnetic field dislocates a vortex core, inducing a circular path [41,42]. Therefore, the alternating field created by the transverse domain wall could explain the core vortex path and the helicoidal domain wall created in wide/narrow nanowire.

### Appendix B. Two interaction field constants FORC distribution parametrization

As seen on Fig. 9(b, c), the FORC distributions obtained for symmetric identical hysterons of coercivity  $\mu_c$  and submitted to two

independent mean interaction fields of constant  $k_{max}$  and  $k_{min}$ , both negative, are constituted of two straight distributions joint on  $H_c$  axis. In order to parametrize this kind of FORC distribution, we defined it through three characteristic points: its lower and higher extremities (points A and B, respectively) and the junction localization on  $H_c$  axis (point C), as denoted on Fig. 9(b). As all points located on the  $H_c$  axis, point C corresponds to hysterons not shifted, i.e.,  $H_u(C) = 0$ , therefore to hysterons reversed back and forth at the system coercivity. Since the magnetization is null in these situations, both mean interaction field values are also null and the point C directly yields the hysterons coercivity  $\mu_c$ , i.e.,  $H_c(C) = \mu_c$ .

The FORC distribution extremities account for the last (point A) and first (point B) hysterons to reverse, near negative and positive system saturation, respectively. More specifically, point B corresponds to a hysteron that reverses down under a reversal field  $H_r = -\mu_c - k_{max}$ , and back up for an applied field  $H = \mu_c - k_{min}$ , where the system magnetization is kept as  $M/M_s = 1$ , for simplicity. Since point A coordinates are identical but using  $M/M_s = -1$ , it yields a FORC distribution symmetrical with respect of  $H_c$  axis. Points A and B coordinates in terms of  $H_c$  and  $H_u$  can be calculated using their respective definitions:

$$H_c(A) = H_c(B) = \mu_c + 0.5(k_{max} - k_{min}) \quad (B1)$$

$$H_u(A) = -H_u(B) = -0.5(k_{max} + k_{min}) \quad (B2)$$

From these equations, one can see that the FORC distribution bending is proportional to the interaction field constants difference, while its extension along  $H_u$  axis is equal to an average interaction field constant.

Finally, with this kind of FORC distribution, one needs only the coordinates of two characteristic points to be able to extract the physical parameters values from an experimental result. The point C localization on  $H_c$  axis yields the hysterons coercivity, while the interaction field constants can be inferred using Eqs. B1 and B2:

$$k_{max/min} = -H_u(A) \pm [H_c(A) - H_c(C)] \quad (B3)$$

### Appendix C. Supplementary data

Supplementary data associated with this article can be found, in the online version, at <http://dx.doi.org/10.1016/j.jmmm.2017.01.071>.

### References

- [1] R.L. White, J. Magn. Magn. Mater. 209 (2000) 1.
- [2] S.S. Parkin, M. Hayashi, L. Thomas, Science 320 (2008) 190.
- [3] L. Thomas, R. Moriya, C. Rettner, S.S.P. Parkin, Science 330 (2010) 1810.
- [4] P.M. Paulus, F. Luis, M. Kroll, G. Schmid, L.J. de Jongh, J. Magn. Magn. Mater. 224 (2001) 180.
- [5] R. López-Ruiz, F. Luis, C. Magén, J. Bartolomé, J. Appl. Phys. 112 (2012) 073906.
- [6] L. O'Brien, D. Petit, E.R. Lewis, R.P. Cowburn, D.E. Read, J. Sampaio, H.T. Zeng, A. V. Jausovec, Phys. Rev. Lett 106 (2011) 087204.
- [7] D.M. Burn, M. Chadha, S.K. Walton, W.R. Branford, Phys. Rev. B 90 (2014) 144414.
- [8] F. Cayssol, D. Ravelosona, C. Chappert, J. Ferré, J.P. Jamet, Phys. Rev. Lett 92 (2004) 107202.
- [9] C. Zinoni, A. Vanhaverbeke, P. Eib, G. Salis, R. Allenspach, Phys. Rev. Lett. 107 (2011) 207204.
- [10] A.S. Esmaily, M. Venkatesan, A.S. Razavian, J.M.D. Coey, J. Appl. Phys. 113 (2013) 17A327.
- [11] M.S. Salem, P. Sergelius, M. Kroll, R.M. Corona, J. Escrig, D. Gorlitz, K. Nielsch, Nanoscale 5 (2013) 3941.
- [12] A. Rotaru, J.H. Lim, D. Lenormand, A. Diaconu, J.B. Wiley, P. Postolache, A. Stancu, L. Spinu, Phys. Rev. B 84 (2011) 134431.
- [13] K. Pitzschel, J. Bachmann, S. Martens, J.M. Montero-Moreno, J. Kimling, G. Meier, K. Nielsch, D. Gorlitz, J. Appl. Phys. 109 (2011) 033907.
- [14] S. Allende, D. Altbir, K. Nielsch, Phys. Rev. B 80 (2009) 174402.
- [15] R. Hertel, J. Kirschner, Phys. B 343 (2004) 206.
- [16] N.M. Han, G.H. Guo, G.F. Zhang, W.B. Song, G.F. Men, Trans. Nonferrous Met. Soc. China. 17 (2007) 1034.
- [17] F. Béron, D. Ménard, A. Yelon, J. Appl. Phys. 103 (2008) 07D908.

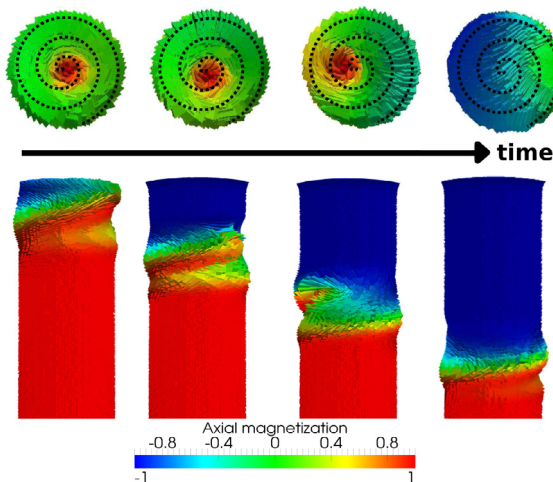


**Fig. 10.** Time evolution snapshots of the helicoidal vortex domain wall propagation. Upper part: Wide extremity top view. The spiral dot line indicates the core path. Lower part: Wide extremity front view.

- [18] H. He, N.J. Tao, in: H.S. Nalwa (Ed.), *Encyclopedia of Nanoscience and Nanotechnology*, vol. 2, American Scientific Publishers, Valencia, USA, 2004, p. 755.
- [19] H. Masuda, K. Fukuda, *Science* 268 (1995) 1466.
- [20] K. Nielsch, F. Muller, A.P. Li, U. Gosele, *Adv. Mater.* 12 (2000) 582.
- [21] K.R. Pirota, D. Navas, M. Hernández-Vélez, K. Nielsch, M. Vázquez, *J. Appl. Phys.* 369 (2004) 18.
- [22] W. Cheng, M. Steinhart, U. Gosele, R.B. Wehrspohn, *J. Mater. Chem.* 17 (2007) 3493.
- [23] I.D. Mayergoyz, *Phys. Rev. Lett.* 56 (1986) 1518.
- [24] F. Béron, L.P. Carignan, D. Ménard, A. Yelon, *Electrodeposited Nanowires and their Applications*, vol. 1, INTECH, 2010, p. 167.
- [25] L.P. Carignan, M. Massicotte, C. Caloz, A. Yelon, D. Ménard, *IEEE. Trans. Magn.* 45 (2009) 4070.
- [26] C.R. Pike, C.A. Ross, R.T. Scalettar, G. Zimanyi, *Phys. Rev. B* 71 (2005) 134407.
- [27] C.I. Dobrota, A. Stancu, *Physica B: Phys. Cond. Matter* 457 (2015) 280.
- [28] J. Escrig, D. Altbir, M. Jaafar, D. Navas, A. Asenjo, M. Vazquez, *Phys. Rev. B* 75 (2007) 184429.
- [29] M.J. Donahue, D.G. Porter, *OOMMF Users Guide*, Version 1.2a3, 2002 <<http://math.nist.gov/oommf>>.
- [30] A. Aharoni, S. Shtrinkman, *Phys. Rev.* 109 (1958) 1522.
- [31] E. Frei, S. Shtrikman, D. Treves, *Phys. Rev.* 106 (1957) 446.
- [32] J. Escrig, J. Bachmann, J. Jing, M. Daub, D. Altbir, K. Nielsch, *Phys. Rev. B* 77 (2008) 214421.
- [33] D. Salazar-Aravena, R.M. Corona, D. Goerlitz, K. Nielsch, J. Escrig, *J. Magn. Magn. Mater.* 346 (2013) 171.
- [34] L. Clime, P. Ciureanu, A. Yelon, *J. Magn. Magn. Mater.* 297 (2006) 60.
- [35] D. Salazar-Aravena, J.L. Palma, J. Escrig, *J. Appl. Phys.* 117 (2015) 193905.
- [36] L.C. Sampaio, E.H.C.P. Sinnecker, G.R.C. Cernicchiaro, M. Knobel, M. Vazquez, J. Velazquez, *Phys. Rev. B* 61 (2000) 8976.
- [37] R. Hertel, *J. Appl. Phys.* 90 (2001) 5752.
- [38] F. Béron, L. Clime, M. Ciureanu, D. Ménard, R.W. Cochrane, A. Yelon, *J. Nanosci. Nanotechnol.* 8 (2008) 2944.
- [39] F. Béron, L.A.S. de Oliveira, M. Knobel, K.R. Pirota, *J. Phys. D* 46 (2013) 045003.
- [40] F. Tejo, N. Vidal-Silva, A.P. Espejo, J. Escrig, *J. Appl. Phys.* 115 (2014) 17D136.
- [41] K.W. Moon, B. Sun, Chun, W. Kim, Z.Q. Qiu, C. Hwang, *Sci. Rep.* 4 (2014) 6170.
- [42] Y.S. Yu, D.S. Han, M.W. Yoo, K.S. Lee, Y.S. Choi, H. Jung, J. Lee, M. Young Im, P. Fischer, S.K. Kim, *Sci. Rep.* 3 (2013) 1301.